Inorganic Ba-Sn Nanocomposite Materials for Sulfate Sequestration from Complex Aqueous Solutions

Journal:	*Environmental Science: Nano*
Manuscript ID	EN-ART-12-2017-001241.R2
Article Type:	Paper
Date Submitted by the Author:	27-Feb-2018

Complete List of Authors:	Levitskaia, Tatiana; Pacific Northwest National Laboratory, Radiochemical Science and Engineering Johnson, Isaac; Pacific Northwest National Laboratory Chatterjee, Sayandev; Pacific Northwest National Laboratory, Energy and Environment Directorate Hall, Gabriel; Pacific Northwest National Laboratory Burton, Sarah; Pacific Northwest National laboratory, Environmental Molecular Sciences Laboratory Campbell, Emily; Pacific Northwest National Laboratory, Radiochemical Science and Engineering Conroy, Michele; Pacific Northwest National Laboratory, Department of Energy; University College Cork National University of Ireland, chemistry Du, Yingge; Pacific Northwest National Laboratory, Environmental Molecular Sciences Laboratory Fujimoto, Meghan; Pacific Northwest National Laboratory, Radiochemical Science and Engineering Varga, Tamas; Pacific Northwest National Laboratory, Environmental Molecular Sciences Laboratory Kruger, Albert; U.S. Department of Energy, Office of River Protection

The presence of high sulfate concentrations in process effluents is problematic for many industries including but not limited to mining and metallurgy, textile, nuclear reprocessing and production of fertilizers. Consequently, removal of sulfate is one of the main challenges in industrial wastewater treatment. One particularly difficult case is the treatment and remediation of legacy nuclear waste produced in large quantities during the cold war era which poses considerable environmental pollution risks. The presence of sulfate in these radioactive streams limit available options for their stabilization in glass wasteforms for safe long-term storage and disposition; and novel methods are needed for sulfate separation or *in situ* sequestration in high-salt multi-component matrices. To develop a convenient and economical option for the selective removal of sulfate from complex carbonate solutions, Ba-Sn nanocrystalline materials were hydrothermally synthesized. This work provides a novel and practical approach to prepare functional inorganic nanomaterials for the separation or *in situ* sequestration of sulfate from aqueous solutions.

Inorganic Ba-Sn Nanocomposite Materials for Sulfate Sequestration from Complex Aqueous Solutions

Isaac E. Johnson, [†] Sayandev Chatterjee, [†] Gabriel B. Hall, [†] Sarah D. Burton, [‡] Emily L. Campbell, [†] Michele A. Conroy, [†] Yingge Du, [‡] Meghan S. Fujimoto, [†] Tamas Varga, [‡] Albert A. Kruger, [§] Tatiana G. Levitskaia[*†]

Organizations

[†]Energy and Environment Directorate, Pacific Northwest National Laboratory, Richland, WA 99354, USA. E-mail: Tatiana.Levitskaia@pnnl.gov

[‡]Environmental and Molecular Sciences Laboratory, Pacific Northwest National Laboratory, Richland, WA 99354, USA

[§] U.S. Department of Energy, Office of River Protection, Richland, WA 99352, USA

Abstract

Selective sequestration of sulfate (SO_4^{2-}) in the form of barite ($BaSO_4$) from alkaline solutions of high ionic strength containing carbonate is problematic due to the preferential formation of $BaCO_3$. Incorporation of sulfate into the insoluble and thermally stable $BaSO_4$ phase can potentially benefit radioactive waste processing by reducing operational challenges and suppressing volatilization of other waste components such as technetium-99. To enhance selectivity of SO_4^{2-} sequestration, a series of **Ba-Sn** nanocomposite materials was prepared using simple hydrothermal synthesis from different Sn(II) and Sn(IV) precursors. Structural characterization indicated that all obtained products predominantly contained $BaSn(OH)_6$ and $Ba_2SnO_2(OH)_4{\bullet}10H_2O$ nanocrystalline phases which were disrupted upon exposure to SO_4^{2-} due to formation of $BaSO_4$. Performance of the **Ba-Sn** materials was tested using complex alkaline solutions simulating radioactive

waste containing 0.094 M SO_4^{2-} and 0.5 M CO_3^{2-} among other constituents. About 54 – 66% of SO_4^{2-} was converted to $BaSO_4$ when a quantity of Ba-Sn material containing approximately a stoichiometric amount of Ba^{2+} relative to SO_4^{2-} was used. In comparison, previous studies indicate negligible $BaSO_4$ formation under similar conditions when a simple Ba^{2+} salt is used. This improvement is attributed to the selective replacement of the stannate by SO_4^{2-}. Thermal stability of the sulfate-loaded product material up to 1100 °C was demonstrated. The obtained materials promise a convenient and economical option for the selective sequestration or removal of SO_4^{2-} from complex carbonate containing solutions.

Introduction

Sulfate is a natural species found in subsurface and ocean water, as insoluble gypsum-like salts. Industrial effluents are responsible for most anthropogenic emissions of sulfate into the environment.[1] Even though sulfate by itself is chemically inert and non-toxic, its high release unbalances the natural sulfur cycle,[2] and removal of sulfate is one of the main challenges in industrial wastewater treatment. Several methods have been proposed for sulfate removal including biological treatment, ion exchange/adsorption, reverse osmosis, electrodialysis, nanofiltration, and chemical precipitation.[3,4] However, none of these technologies are applicable for the treatment of complex brine-like wastes containing sulfate at lower concentrations than other common inorganic anions including nitrate, nitrite, carbonate, aluminate, phosphate, chromate and others on the industrial scale. One example of such waste streams is the large quantities of legacy radioactive waste which are stored in the underground tanks at the U.S. Department of Energy (DOE) Hanford site. Removal of sulfate from the nuclear tank waste has been considered, and several technologies have been tested including ion exchange,

solvent extraction, and chemical precipitation, however no practical solution has been found to date.[5]

The current approach for the long-term storage and disposition of low-level and low-activity nuclear waste relies mainly on immobilization in borosilicate glass and cementitious waste forms. The presence of sulfate in the Hanford waste poses significant complications in implementation of the vitrification and grouting processes and negatively impacts performance of the final waste form. In the case of cementitious materials, sulfate incorporation promotes changes in waste-form microstructure that may cause a loss of waste form integrity through expansion and/or cracking, resulting in the potential release of stored radionuclides to the environment.[6-9] During vitrification of the nuclear waste, sulfate acts as a poison generating considerable process challenges related to its low solubility in the borosilicate glass and formation of an immiscible sulfate salt layer on top of the melt. This results in limited waste loading into the borosilicate glass waste form matrix, may have negative impact on melter operability (e.g., possibly creating corrosion problems and short-circuiting electrical equipment), increase burden on off-gas processing, and potentially hinder incorporation of some volatile waste constituents including radioactive technetium-99 (Tc) into the glass matrix.[10,11] Recent studies have suggested a correlation between concentration of sulfate in waste and retention of Tc in the glass melt [12] and have led to the hypothesis that incorporation of sulfate into a thermally stable phase that is inert to reactions in a melter to at least 800 °C may diminish its effect on Tc volatility during vitrification.

One approach is to sequester sulfate in the waste matrix in the form of barite ($BaSO_4$), which has low aqueous solubility with a K_{sp} of 1.08×10^{-10} (25 °C)[13] and is compatible with the borosilicate glass. However, sequestration through addition of a soluble Ba^{2+} salt such as nitrate or chloride to the waste matrix with the purpose of sulfate sequestration as $BaSO_4$ is problematic due to the presence of high concentrations of carbonate and chromate, both forming

low solubility $BaCO_3$ and $BaCrO_4$ salts with the respective K_{sp} of 8.1×10^{-9} and 2.4×10^{-10} (25 °C)[13] which are similar to that of $BaSO_4$. This necessitates a large stoichiometric excess of Ba^{2+} over sulfate to achieve its effective precipitation. Indeed, chemical precipitation of sulfate using barium has been recognized as an effective method for waste stream treatment for many years,[14,15] but was found to be poorly suited for the treatment of the alkaline nuclear waste such that either waste acidification or addition of Ca^{2+} is required to remove bulk carbonate prior to $BaSO_4$ precipitation.[16] A possible solution is to facilitate selective sequestration of sulfate with Ba^{2+} by supplying it in a different chemical form which promotes selective reaction with sulfate in the presence of high carbonate concentrations as compared with the simple Ba^{2+} salt. Engineered inorganic functional materials with layered structural frameworks have previously been employed to address similar issues related to selective sequestration of other inorganic ions of interest. A representative example is highly selective removal of TcO_4^- from a multicomponent alkaline high ionic strength solutions typifying the matrix of tank waste using a redox-active Sn(II/IV) based alumino-phosphate composite enabling its selective uptake and reduction to Tc(IV).[17] The selective removal of anions of iodine (I^-, IO_3^- and IO_4^-) has also been demonstrated from multicomponent matrices present in Hanford groundwater using bimetallic composites consisting of borderline soft, redox-active transition metals such as Co^{2+} and Cr^{3+}.[18] The material was configured in a hydrotalcite-like layered double hydroxide (LDH) structure to provide a large enough surface area for enhanced uptake efficiency. Recent studies have demonstrated that LDH materials represent a valuable option for separation of radioactive and toxic contaminants from a variety of waste streams.[19-23]

This suggests that similar clay-like LDHs may offer an attractive option to achieve desirable selectivity for sulfate by introducing an ion exchange step prior to reaction with Ba^{2+}. They

originate from hydrotalcite $[Mg_6Al_2(OH)_{16}]CO_3 \bullet 4H_2O$, and substitution of Mg^{2+} and Al^{3+} by other divalent, trivalent or tetravalent metal ions resulting in a large class of isostructural materials with physicochemical properties that can be tailored to achieve a desirable property of interest. However, because of the structural constraints large metal ions do not readily form LDH compounds prohibiting generation of this structure for Ba^{2+}. Among alkaline earth cations besides Mg^{2+}, only Ca^{2+} with the ionic radius of 0.10 nm forms sufficiently stable LDH materials, and many relevant examples of Ca-Al hydrotalcites with various interlayer anions have been reported.[24-26] Sr^{2+} and Ba^{2+} with respective radii of 0.113 and 0.136 nm[27] are too large to form LDH structure. The only synthetic Ba^{2+}-Fe^{3+} hydroxide LDH-like material was obtained under forcing conditions of extremely high $[OH^-]>10$ M concentration.[28,29] Even though a few reports suggested formation of Ba^{2+}-bearing hydrotalcite phase under mild chemical conditions, the experimental evidence of the formation of Ba^{2+}-bearing hydrotalcite remains ambiguous.[30-32] In this work, we evaluated whether Ba^{2+}-based double metal hydroxides, close LDH relatives, of the general structure $M^{2+}M^{4+}(OH)_6$ may offer potential solution.

Barium hexahydroxidostannate(IV) $BaSn(OH)_6$, easily prepared by hydrothermal or similar synthesis, is known for its use as a precursor for $BaSnO_3$ perovskite.[33] Non-hydrated $BaSn(OH)_6$ prepared by hydrothermal synthesis using $BaCl_2$ and $K_2Sn(OH)_6$ at 100 °C followed by air drying yielded a crystalline structure with a CsCl-like arrangement of the Ba^{2+} cations occupying eight-coordinate sites and $Sn(OH)_6^{2-}$ anions connected through hydrogen bonding to form a three-dimensional framework.[34] Furthermore, single crystal X-ray diffraction of the hydrated $BaSn(OH)_6 \bullet 5H_2O$ obtained by either the slow diffusion of aqueous solutions of $Na_2Sn(OH)_6$ and $Ba(NO_3)_2$ or recrystallisation of freshly prepared $BaSn(OH)_6 \bullet nH_2O$ at ambient conditions adopted a layered structure comprised of two octahedral $Sn(OH)_6^{2-}$ ions and two

monocapped square antiprisms of $Ba(OH)_4(H_2O)_5$, octahedral $Sn(OH)_6^{2-}$ ions and 5 water molecules occupy the space between layers.[35] While this layered arrangement is not identical to that of hydrotalcite, the similarities in their structures highlight the importance of the hydration water and encourage potential utilization of $BaSn(OH)_6$ for applications considered as traditional for the LDH materials. Therefore, it was of interest to explore if the layered $BaSn(OH)_6 \cdot 5H_2O$ or other layered $Ba_{1+x}SnO_{2x}(OH)_{6-2x} \cdot nH_2O$ structures could introduce a preferential sulfate selectivity based on the preferential exchange of the interlayer $[Sn(OH)_6]^{2-}$ anion with highly hydrated sulfate as an initial vector for preferential formation of $BaSO_4$. Toward this objective, a series of **Ba-Sn** materials was prepared containing non-hydrated $BaSn(OH)_6$ and $Ba_{1+x}SnO_{2x}(OH)_{6-2x} \cdot nH_2O$ at different relative ratios which were tested for sulfate sequestration in the simulated tank waste solutions.

Experimental

Materials

$BaCl_2 \cdot 2H_2O$ (99.8%) was obtained from Baker and Adamson. $SnCl_2$ (anhydrous, 98%) and $SnCl_4 \cdot 5H_2O$ (98%) were purchased from International Laboratories (IL). SnO (97%) and NaOH (50 wt%) were obtained from Sigma Aldrich. All other chemicals (reagent grade) were purchased from the Sigma Aldrich, Alfa Aesar, or Baker & Adamson Chemicals and used without further purification. Distilled deionized (DI, ≥18 MΩ) water was used for the preparation of the aqueous solutions.

Synthesis of Ba-Sn composites

Synthesis of the Ba-Sn composites was performed by hydrothermal method using modifications to a procedure reported elsewhere[36] from $BaCl_2 \cdot 2H_2O$ and three different Sn precursors including $SnCl_2$, a mixture of $SnCl_2$ and $SnCl_4 \cdot 5H_2O$ (at a 2:1 molar ratio),

and SnO at a starting molar ratio of Ba:Sn of 3:1. The resulting products are referred in the text as **Ba-SnCl$_2$**, **Ba-SnCl$_{2/4}$**, **Ba-SnCl$_4$** and **Ba-SnO**, respectively, or jointly as **Ba-Sn**. In a typical procedure, $BaCl_2$ (0.006 mol) was dissolved in 20 mL of DI water and the solid Sn precursor (0.002 mol) was added followed by addition of water for a total approximate volume of 50 mL. The suspension was stirred for approximately 15 minutes and the pH was adjusted from the initial value of 1-2 to the target pH of 12.8-13.0 using NaOH solution. The pH of the solution was measured using an ORION™ 8103BNUWP Ross Ultra™ Semi-Micro Glass pH electrode calibrated with the ORION pH 4.01 and pH 10.01 standard buffers. The calibration check was performed with the ORION pH 7.00 and pH 12.46 standard buffers. After adjusting the pH, the solution was covered with Parafilm® and magnetically stirred at 150-250 rpm for 3 days. This aging step was applied to increase number of nucleation sites and achieve uniformly-sized microcrystalline structure of the final product.[36] The pH of the solution was monitored daily and adjusted up to the target pH as needed. The reaction mixture containing precipitated solids and aqueous supernatant was then placed in a Teflon-lined autoclave (Parr Instrument Company, Moline, IL) and kept at 110 ± 5 °C for 72 hours to yield the crystalline aggregate product. The reaction mixture was then cooled overnight and the **Ba-Sn** material was gravimetrically filtered using Whatman filter paper (ashless, grade 40, 110 mm diameter), and rinsed with an excess of DI water until neutral pH of the rinse was achieved. The obtained **Ba-Sn** materials were then air dried, ground into a homogenous powder using a mortar and pestle, and stored in 1-2 dram Kimble Chase Opticlear borosilicate glass vials. The metal composition of the composites was examined using Inductively Coupled Plasma Optical Emission Spectroscopy (ICP-OES) by dissolving massed amounts of the composite in 2.7 M HNO_3. The elemental inorganic carbon analysis was conducted by Atlantic Microlab, Inc. (Norcross, GA).

Test Solutions

The efficiency and kinetics of sulfate and/or chromate uptake by the obtained **Ba-Sn** composites was examined initially using simple solutions containing 85 mM Na_2SO_4 or Na_2CrO_4 in 0.5 M NaOH and/or 1 M $NaNO_3$ followed by testing in a complex solution simulating low activity waste (LAW), the Hanford AN-102 tank, with the composition listed in Table S1. The composition of the AN-102 LAW simulant was referenced from Jin et al.[11] The components in the AN-102 LAW simulant were added in the order as referenced from Jin et al. with the exceptions that the NiO, PbO, and SiO_2 were excluded, and the Na_2SO_4 was added last. Each chemical in the simulant was allowed to fully dissolve before the next component was added. The simulant settled for several days and was then filtered. The original simulant contained 11.8 ± 0.4 mM Na_2CrO_4 and 94 ± 3 mM Na_2SO_4. The final simulant composition was analyzed by ICP. To examine performance of the **Ba-Sn** composites at variable sulfate concentration, the same simulant samples containing 27 ± 1 and 60 ± 2 mM Na_2SO_4 were also prepared.

Batch contact experiments

Typical sample preparation involved rigorous mixing of the solid **Ba-Sn** material suspended in the test solution in a ½ dram vial so that the ratio of the weight of the sorbent to the solution volume was 12 – 50 mg mL^{-1} under stirring. Samples were centrifuged for 3 minutes at 1500 rpm, supernatant transferred to a new Opticlear glass vial and the anion uptake quantified by Raman spectroscopy. Raman measurements were performed using an InPhotonics RS2000 high-resolution spectrometer equipped with a thermoelectrically cooled charged coupled device (CCD) detector operating at -52 °C, a 670.974 nm 150 mW diode laser as the excitation source; and focused fiber optic probe RamanProbeTM operated in a 180° back reflection mode. An integration time of 10 s was used for each acquisition, and 10 scans were acquired and

averaged for each sample. Spectra of the simulant of individual samples were collected with the laser pointing through the side of an Opticlear glass vial. The spectra were averaged, baseline corrected using OMNIC 6.2 software, and normalized to the maximum wavenumber of the water band. Additional localized baseline corrections for anion peaks of interest and normalization to the water band after were done in order to accurately baseline spectra for analysis as needed. The Raman intensity of the SO_4^{2-} band[37] at 983 cm^{-1} or CrO_4^{2-} band[37] at 848 cm^{-1} in the initial test solutions were compared to the intensities of the corresponding bands at each time point from 10 min to 60 hrs and used to quantify the anion uptake by the **Ba-Sn** materials.

Characterization Techniques

The structural and morphological features of the **Ba-Sn** materials as prepared and after uptake of sulfate and/or chromate from the test solutions were examined by a range of spectroscopic and microscopic techniques. To prepare loaded samples for diffraction, microscopy and spectroscopic studies, ~150 mg of the composite material was contacted with 6 mL of the test solution under agitation at room temperature. After 24 hours the liquid phase was removed from the sample by centrifugation and decantation, and the loaded composite was rinsed with DI water (5x10 mL) and air-dried at room temperature until completely dry.

X-ray Diffraction (XRD) was conducted using a Philips X'pert Multi-Purpose Diffractometer (MPD) (PANAlytical, Almelo, The Netherlands) equipped with a fixed Cu anode operating at 45 kV and 40 mA. XRD patterns were collected in the 5–100 2q-range with 0.04 steps at a rate of 5 s per step. Phase identification was performed using JADE 9.5.1 (Materials Data Inc.) and the 2012 PDF4+ database from ICSD.

SEM measurements were performed with a FEI (Hillsboro, OR, USA) Helios 660 NanoLab™ dual-beam Scanning Electron Microscope (SEM) with a Focused Ion Beam (FIB) equipped with

an EDAX (EDAX Inc., Mahwah, NJ) compositional analysis system. Samples for both SEM and TEM were deposited as fine powders onto a holey carbon copper-grid. In the SEM, imaging was performed in transmission High Angle Annular Dark Field (HAADF) mode (using the FEI STEM-3+ detector) and with secondary electron imaging. Selected specimens were ion-beam sectioned using the SEM-FIB and mounted on Omniprobe lift-out grids (Electron Microscopy Sciences, Hatfield, PA) for analysis in the Transmission Electron Microscope. TEM work was performed using a JEOL ARM200F (JEOL, Peabody, MA) operated at 200 keV and equipped with a Noran™ (Thermo Scientific, Waltham, MA) EDS system and a FEI Titan 30-800 operated at 300 keV and equipped with a Gatan™ (Gatan, Inc., Pleasanton, CA) Image Filter. Diffraction patterns and electron micrographs were analyzed with Gatan Digital Micrograph™ 3.01 and aided with simulated diffraction patterns generated using CrystalMaker®2.2, a crystal and molecular structures program for Mac and Windows, and SingleCrystal®2.0.1, an electron diffraction simulation program distributed by Crystal Maker Software Ltd., Oxford, England (http://www.crystalmaker.com).

Fourier Transform Infrared Spectroscopy (FTIR) measurements were conducted using a spectrometer (ALPHA model, Bruker Optics) equipped with platinum attenuated total reflectance (ATR) module with a single reflection diamond plate and clamp, and operated with OPUS software (Version 6.5, Build 6.5.92). Samples were measured by placing a small amount of powder on the diamond plate, clamping the powder down and then taking the measurement. Each sample was run at ambient conditions (22 ± 2 °C), the final spectra produced was an average of 32 scans with a resolution of 4 cm^{-1}. Background measurements at ambient conditions of air were taken prior to each sample. The plate and clamp were cleaned with DI water after each sample.

Solid-state ^{119}Sn NMR experiments were run on a 300 MHz Inova spectrometer. A 4mm HXY Chemmagnetics style

probe was used. The samples were spun at 14 kHz to avoid spinning sidebands. The pulse sequence was a 45 deg rf pulse with 10 ms acquisition time and the pulse delays ranged from 30 to 120 sec. Depending on the sample, 8,000 – 12,000 scans were collected. The data were processed using Mnova software (Mestrelab Research, S.L. Escondido, CA).

X-ray Photoelectron Spectroscopy (XPS) data were recorded on a Phi5000 Versa Probe system equipped with a monochromatic Al Ka X-ray source (1486.7 eV) and a hemispherical analyzer. Powder samples were mounted using double-sided carbon conductive tape attached to a stainlesssteel sample holder. The instrument was calibrated for Cu ($2p_{3/2}$) at 932.6 (0.1 eV) with the FWHM (full with at half maximum) of 0.98 eV. The surface charge was eliminated by charge neutralizer and correction of data referencing the 284.5 eV C 1s peak. The percentages of individual elements detected were determined from the relative composition analysis of the peak areas of the bands on the basis of the relative peak areas and their corresponding sensitivity factors to provide relative compositions. XPS peak fitting was done using the software XPSPEAK41 (University of Warwick, Coventry, UK) with Shirley type background and 20% GL (Gaussian–Lorentzian ratio).

Thermal Gravimetric/Differential Thermal Analysis (TG/DTA) data was collected using a SDT Q600 (TA Instruments) analyzer. The thermocouple was calibrated with 4 pure metals (indium, zinc, aluminum, and gold). The DTA baseline was run with empty beams and the TGA baseline (beam expansion) was calibrated with alumina reference weights supplied by TA Instruments vendor. The untreated and AN-102 simulant treated **Ba-Sn** samples were run with an alumina oxide reference. Air was flowed over the samples at a rate of 50 mL/min. The **Ba-SnO** composite untreated and AN-102 treated were run with an air flow rate of a 100 mL/min. The sample masses were ~ 15 mg and the

temperature was ramped from (22 ± 3°C) to 1100°C at a rate of 10°C min^{-1}.

3.0 Results and Discussion

Ba-Sn Materials Synthesis and Characterization

The preparative methods reported in the literature for the synthesis of the $BaSn(OH)_6$ materials typically utilize Sn(IV) precursors of $Sn(OH)_6^{2-}$[34] or $SnCl_4$.[38,39] The significantly different ionic radii of Sn^{2+} (0.093 nm) and Sn^{4+} (0.069 nm) which potentially may promote formation of different crystalline products as well as redox mobility of the Sn(II)/Sn(IV) couple prompted us to evaluate the effect of the nature of Sn starting materials on the reaction product. Synthesis of the **Ba-Sn** materials was performed using the same $BaCl_2$ starting compound and four different Sn precursors including SnO, $SnCl_2$, a $SnCl_2/SnCl_4$ mixture, and $SnCl_4$ at pH 12.8 – 13. It is likely that during hydrothermal synthesis Sn(II) is oxidized to Sn(IV), and therefore the $SnCl_2$, $SnCl_2/SnCl_4$ mixture and $SnCl_4$ precursors were tested to examine the effect of the Sn oxidation state in the starting compound on the reaction pathway. In addition, it was in our interest to test whether the Sn salt and oxide precursors will generate different products, and to compare the performance of the obtained materials toward sulfate uptake from the complex mixtures. The Ba:Sn molar ratio of 3:1 was used to ensure excess of Ba^{2+} and reduce the possibility of SnO_2 formation. Synthesis was conducted in air to examine if the presence of CO_2, leading to possible barium carbonate precipitation, would interfere with the formation of $BaSn(OH)_6$. This approach provides important information on the robustness of the synthetic procedure using various Sn precursors when performed under aerated conditions.

Sharp reflections in the X-ray diffractograms indicate high

crystallinity of the **Ba-Sn** materials (Figure 1A). Marked similarities are observed in the diffractograms of all obtained materials suggestive of common key crystallographic phases generated irrespective of the Sn(II/IV) starting material. The diffraction patterns resemble a combination of a non-hydrated $BaSn(OH)_6$ phase[38] and $Ba_2SnO_2(OH)_4 \bullet 10H_2O$[40] with possible minor fraction of the hydrated $BaSn(OH)_6 \bullet 5H_2O$.[35] To further validate formation of $BaSn(OH)_6$, the **Ba-SnO** material was subjected to analysis by single crystal x-ray diffraction. The determined lattice (monoclinic, $P21/n$, a = 9.3969(6) Å, b = 6.3358(4) Å, c = 10.5655(7) Å, β = 113.174(21)°) was found to be nearly identical to one of anhydrous $BaSn(OH)_6$ reported by Mizoguchi et al.[34]

While anhydrous $BaSn(OH)_6$ is the dominant phase in the Ba-SnO sample, the relatively significant quantities of the hydrous $BaSn(OH)_6 \bullet 5H_2O$ and $Ba_2SnO_2(OH)_4 \bullet 10H_2O$ phases were found in the **Ba-SnCl$_{2/4}$** and **Ba-SnCl$_4$** products. These trends indicate that the SnO precursor promotes formation of the non-hydrated $BaSn(OH)_6$ phase which was attributed to the low solubility and high stability of SnO romarchite toward aqueous hydrolysis under alkaline conditions[41] allowing its direct participation in the hydrothermal reaction. Conversely, $SnCl_4$ exhibits high tendency toward hydrolysis and dominant formation of $Sn(OH)_6^{2-}$ at pH>10[42] facilitating formation of the $BaSn(OH)_6 \bullet 5H_2O$ and $Ba_2SnO_2(OH)_4 \bullet 10H_2O$ products.

It was observed that the first diffraction peak positions of **Ba-Sn** composites exhibit small differences (Figure 1A). To be specific, the first diffraction peak position of **Ba-SnO** is located at a higher region than the other three. This phenomenon was attributed to the different amount of interlayered carbonate in these samples. All materials also contain small amounts of the additional phase corresponding to $BaCO_3$, atmospheric CO_2 dissolved in the alkaline synthetic mixtures being the source of carbonate. **Ba-SnO** and **Ba-SnCl$_2$** samples contained the smallest and the largest

quantity of $BaCO_3$ respectively.

Elemental ICP analysis of the obtained products demonstrated that the molar ratio of Ba:Sn was similar in all materials and resided in the 1.4 – 1.7 range. Consistent with the XRD results, the excess of Ba over an equimolar amount of Ba:Sn expected for the $BaSn(OH)_6$ product was attributed to the formation of $Ba_2SnO_2(OH)_4 \bullet 10H_2O$ and $BaCO_3$ phases. Formation of the latter is confirmed by the carbon elemental analyses showing that inorganic carbon constituted 0.22, 0.32, 0.70, and 1.3 wt% for the **Ba-SnO**, **Ba-SnCl$_4$**, **Ba-SnCl$_{2/4}$**, and **Ba-SnCl$_2$** samples, respectively.

The IR spectra of the obtained **Ba-Sn** materials exhibit similar profiles (Figure 2A). Lattice vibrations corresponding to the Ba – O – Sn network are evident in overlapping 400 – 600 cm^{-1} peaks; a strong band at about 500 cm^{-1} was identified as the Ba-OH vibration[43] while weaker peaks at 500 – 600 cm^{-1} were attributed to the Sn-O and Sn-OH vibrations.[44] All materials exhibited a nearly identical set of bands at about 855, 1060, and 1455 cm^{-1} corresponding to $BaCO_3$[45] as well as interlayer carbonate.[46] Consistent with elemental analysis and XRD results, comparison of the carbonate band intensities indicates that the amount of carbonate in the samples increases in the order **Ba-SnO** << **Ba-SnCl$_4$** < **Ba-SnCl$_{2/4}$** < **Ba-SnCl$_2$**. The band at around 1635 cm^{-1} and very broad and poorly defined band at 3443 cm^{-1} are attributed to the O-H bending and stretching, respectively from interlayer water.[46] Sharp features at about 3400 cm^{-1} are assigned to the stretching vibration of the hydroxide in $BaSn(OH)_6$.[34]

The **Ba-SnO** sample was further evaluated with electron microscopy. The representative images show lath-like elongated hexagonal structures (Figure 3A). Elemental mapping of the laths shows a near uniform distribution of Ba along the skeletal framework. Carbon and oxygen almost equally distributed along the skeletal framework, suggesting that the CO_3^{2-} anion might be

closely associated with the Ba center. This is noteworthy as $BaCO_3$ is not observed as a dominant phase in the diffractogram of this material, suggesting that CO_3^{2-} might be an interlayer anion in the $Ba_2SnO_2(OH)_4$•$10H_2O$ framework. Elemental mapping also shows that the distribution of Sn along the skeletal framework nearly maps that of Ba. This is presumably suggestive that Sn is closely associated with Ba. The quantitative elemental distribution determined by Energy Dispersive X-ray Spectroscopy (EDS) showed a Ba:Sn atomic ratio of 1.6:1 which agrees well with ICP-OES data, which indicated the Ba-Sn ratio as 1.4:1. This is consistent with the two major phases being $BaSn(OH)_6$ and $Ba_2SnO_2(OH)_4$•$10H_2O$.

Collected transmission electron micrographs shown in Figure 3A, revealed that the samples were primarily crystalline in nature with small inclusions of amorphous material as reflected by the SAED on the represented area. However, the diffractogram is not matched by any simple Ba-only systems such as $BaSO_4$, $BaCO_3$, $Ba(OH)_2$ or binary Ba-Sn species such as Ba_2SnO_4, $BaSnO_3$ or $BaSn(OH)_6$•$5H_2O$. This suggests a possible change in the structural integrity of the crystalline phases under the electron beam; this phenomenon is likely to affect the lattice of $Ba_2SnO_2(OH)_4$•$10H_2O$ containing water and hydroxide prone to their loss in presence of the electron beam.

Photoelectron spectroscopy was used to observe the electronic environment of the Ba, Sn, O, and S elements comprising the **Ba-SnO** material (Figure 4). The Ba 3d region of the XPS spectrum exhibits a doublet with low energy $3d_{5/2}$ line centered at 779.9 eV. This value is consistent with the binding energy of 779.8 eV observed in $BaSnO_3$ perovskite.[47,48] The narrow profile of the band indicates similar electronic environment of Ba^{2+} in $BaSn(OH)_6$ and $Ba_2SnO_2(OH)_4$•$10H_2O$. The Sn 3d region of the phototelectron spectrum of the **Ba-SnO** material prior to anion exposure, shows a characteristic doublet with the dominant peak of the low energy $3d_{5/2}$ line centered at 486.4 eV.

The binding energy value falls in the lower end of values observed for pure Sn(IV) compounds such as SnO_2 which vary from 487.3 eV[49] to 486.1 eV.[50,51] This is not totally unexpected for an electron rich Sn(IV) species consisting of σ-donating OH^- groups. Further, studies by Kwoka *et al.* have shown that Sn(IV) can occur in perovskite structures with binding energies ~486.6 eV.[52] Similar studies on the valence of Sn in Sn-grafted TiO_2, Sn-grafted Ru/TiO_2 and Sn, Ni-grafted TiO_2 also show Sn(IV) binding energy values to fall in that region.[53-55] The comparison of our data with these previous reports clearly demonstrates that the valence state of Sn in the **Ba-Sn** materials is +4. The fitting of the Sn $3d_{5/2}$ band confirms the dominance of a Sn species with a chemical environment equivalent to the Sn electron binding energy in the $BaSn(OH)_6$ and $Ba_2SnO_2(OH)_4$•$10H_2O$ environments. A small fraction of lower valent Sn(II) with a Sn $3d_{5/2}$ binding energy value of 488 eV is also observed in the composite, presumably due to some impurities present in the reactants or due to chemical reduction during the synthetic step. However, the fraction of this Sn(II) species is low enough to not be of any concern for subsequent steps. The O 1s spectral region is dominated by a broad peak that can be fitted to the peaks with binding energies of 531.2 eV as the dominant band and a shoulder at 532.1 eV (Figure 4 bottom left) ascribed to the respective lattice oxygen, and adsorbed or solvated water in accord with the literature observations for the perovskite-like structures of the form $MSnO_3$ (M = Ca, Sr, Ba).[48,56]

To get better insight into Sn coordination environment in the obtained **Ba-Sn** materials, ^{119}Sn NMR measurements were performed. ^{119}Sn NMR spectra of a SnO_2 reference and **Ba-Sn** materials synthesized from multiple source materials are presented in Figure 5. The SnO_2 reference material was set to a literature isotropic chemical shift (δ_{iso}) of -604 ppm and displayed a single relatively sharp resonance.[57,58] It was observed that all **Ba-Sn** products contain Sn in more than one coordination environment. Single crystals formed during the synthesis of the **Ba-SnO** material

and manually separated from the bulk material exhibited a single resonance at δ_{iso} = -581 ppm. In concert with single crystal XRD analysis confirming their $BaSn(OH)_6$ identity, this measurement provided a definitive assignment to the resonance at -581 ppm.[34] The bulk material obtained from synthesis with a SnO precursor showed one ^{119}Sn resonance centered around -583 ppm attributed to the $BaSn(OH)_6$, and a second resonance at -572 ppm attributed to $Ba_2SnO_2(OH)_4{\bullet}10H_2O$. Materials synthesized from starting materials of $SnCl_2$, $SnCl_4$ and a mixture of $SnCl_2$ and $SnCl_4$ showed similar spectral profiles with a broad resonance centered at -579 to -583 ppm and overlapping with the second broad resonance appearing between -571 and -572 ppm, albeit the ratio of these resonances changed depending upon Sn source material. This suggests two Sn environments which form preferentially depending on Sn source material, and in agreement with the aforementioned powder XRD provides assignment to the second Sn environment as $Ba_2SnO_2(OH)_4{\bullet}10H_2O$. It should be noted that no presence of unreacted Sn precursors was observed in any spectra of the product materials.

The thermogravimetric analysis (TGA) and differential thermal analysis (DTA) of the as synthesized **Ba-Sn** materials demonstrated overall similar thermal behavior (Figures 6A, S1-S3). As heating begins there is an endotherm centered around 91 °C which is accompanied by a 12 % mass loss in the TGA. This event is believed to be the loss of interstitial water in the $Ba_2SnO_2(OH)_4{\bullet}10H_2O$ fraction of the material. A second endotherm centered around 265 °C is accompanied by a 9 % mass loss in the TGA. The temperature of 265 °C is in good agreement with literature reports of 260-270 °C as the temperature necessary to form barium stannate ($BaSnO_3$) from $BaSn(OH)_6$ and the hydrates thereof.[33,38,39,59] An exotherm is present at 665 °C accompanied by a small mass loss of around 1 % and is attributed to the decomposition of carbonate. The integrity of the crystalline phase separated from **Ba-SnO** material upon heating to 1100 °C

was also probed by IR spectroscopy (Figure 2B). A significant change is observed in the infrared spectrum with a shift of the band corresponding to the Ba-(OH)-Sn moiety at approximately 485 cm^{-1} shifting to approximately 610 cm^{-1} due to conversion to barium cassiterite. This is consistent with a stronger M-O bond upon removal of H from the μ-bridging hydroxides. Dehydration of the interlayer H_2O from $Ba_2SnO_2(OH)_4 \bullet 10H_2O$ is also observed via the disappearance of peaks at 1624 cm^{-1} and 2,800-3,600 cm^{-1}.

Kinetics of SO_4^{2-} and CrO_4^{2-} uptake from simple solutions

Performance of the obtained **Ba-Sn** materials for the uptake of SO_4^{2-} or CrO_4^{2-} anions was initially evaluated using simple alkaline solutions containing 85 mM of the target anion (SO_4^{2-} or CrO_4^{2-}) in the 0.5 M NaOH matrix. The kinetics of the anion uptake was monitored over 48 hours by Raman spectroscopy. In these batch experiments, ~25 mg of composite was contacted with 1 mL of the test solution. The uptake of SO_4^{2-} or CrO_4^{2-} with time was quantified by the reduction of the intensity of the corresponding Raman band at 983 cm^{-1} and 848 cm^{-1}, respectively. Two distinct uptake regimes were observed. About 60% of SO_4^{2-} or CrO_4^{2-} was removed from the simple solutions within a few minutes after contacting it with Ba-Sn materials; because of this nearly instantaneous uptake, reliable kinetic parameters could not be obtained. In the second regime, the equilibrium was approached within ~12 hours and showed ~76 – 83% uptake by mass for both anions (Table 1 and Figure 7). These uptake kinetics observed for the **Ba-Sn** composites is similar to the performance of the layered Sn-Al-phosphate material previously developed for the sorption of Tc-99.[17] It should be noted that the Cr(VI) was not reduced to Cr(III) during contacts and was sequestered as Cr(VI), which is consistent with the Sn from the composite being present in +4 oxidation state and therefore cannot act as a reductant for Cr(VI).

Characterization of the Ba-Sn materials exposed to the sulfate and chromate alkaline solutions

Treatment of the **Ba-Sn** materials with either SO_4^{2-} or CrO_4^{2-} alkaline test solutions resulted in complete structural change in the lattice framework, the most prominent being the complete disruption of the Ba-O-Sn frameworks, as shown in the XRD diffractograms of the anion exposed materials in Figure 1B. This is accompanied by the generation of complex diffractograms consistent with formation of multiple phases. The diffractograms are dominated by a phase resembling $BaSO_4$ in the case of the SO_4^{2-} treated material and a $BaCrO_4$ like phase in the case of the CrO_4^{2-} treated material.

The IR spectra for the **Ba-Sn** materials treated with simple alkaline solutions of either chromate or sulfate are shown in Figures 2B and S4 – S6. Exposure to a simple alkaline solution containing CrO_4^{2-} resulted in a near elimination of the band at 485 cm^{-1}, and the appearance of three large bands corresponding to CrO_4^{2-} appeared at 841, 885, and 895 cm^{-1}.[60] Additionally in the post exposure material, a peak appeared at 415 cm^{-1} attributed to the Ba-O vibration.[61] Exposure of the **Ba-Sn** materials to a simple alkaline solution containing SO_4^{2-} in the absence of CrO_4^{2-} also resulted in elimination of vibrational bands associated with the original materials, however the emergent bands differed greatly. In particular, a pair of bands appeared at 603, and 632 cm^{-1}, as well as three bands at 982, 1056, 1118 and 1184 cm^{-1}. These agree reasonably with literature spectra of $BaSO_4$ exhibiting vibrations at 610, 637, 984, 1075, 1123, and 1187 cm^{-1}.[62]

The morphological and spatial changes in the materials upon SO_4^{2-} or CrO_4^{2-} exposure were studied through electron microscopy. The representative microscopic images of the **Ba-SnO** composites upon exposure to SO_4^{2-} demonstrate near uniform Ba distribution throughout the skeletal framework analogous to the unexposed materials (Figure 3B). There is nearly quantitative mapping of S with Ba at the expense of a significant lowering of Sn along the framework. This is consistent with the XRD showing $BaSO_4$ as the dominant phase. Exposure of the composite to CrO_4^{2-}

results in similar changes with Cr distribution tracking nearly quantitatively with Ba at the expense of Sn. This is consistent with XRD results showing a dominance of the $BaCrO_4$ phase. Notably, elemental mapping demonstrates almost complete disappearance of Sn from the exposed materials. The collected TEM micrographs of both the SO_4^{2-} and CrO_4^{2-} loaded composites also revealed the samples to be primarily crystalline, with the diffractograms in the SAED being different from the precursor composite, confirming annihilation of the original crystalline framework, and suggesting complete structural change upon exposure to either SO_4^{2-} or CrO_4^{2-}. The diffractogram patterns are again not consistent with the expected simple Ba-only systems such as $BaSO_4$, $BaCO_3$, $Ba(OH)_2$ or $BaCrO_4$ as seen in the powder XRD studies. This is again suggestive of the presumable disintegration of the samples under the electron beam.

The results of the XPS measurements of the representative **Ba-SnO** material treated with either SO_4^{2-} or CrO_4^{2-} alkaline solutions are shown in Figure 4. Exposure of the material to SO_4^{2-} resulted in the binding energy of Ba $3d_{5/2}$ line to raise from 779.9 to 780.4 eV, which is consistent with the formation of $BaSO_4$.[63] On the other hand, exposure to CrO_4^{2-} slightly lowered the binding energy to 779.6 eV, this value being similar to that for $BaCrO_4$.[64] The Sn $3d_{5/2}$ spectral line of the **Ba-SnO** material exposed to either SO_4^{2-} or CrO_4^{2-} in simple simulant was observed to slightly decrease the binding energy from 486.5 to 486.3 eV, suggesting that the chemical environment around the Sn center became more electron rich. The O 1s region of the spectrum showed significant changes for the treated material. Exposure to SO_4^{2-} in simple simulant results in shifting the binding energy of the dominant band to 532 eV, with a shoulder at 533.5 eV. The line at 532 eV is consistent with O 1s line from a $BaSO_4$ species.[65] The S 2p region of the spectrum showed a dominant peak at 168.9 eV, which can be attributed to $BaSO_4$ species.[65] Exposure to CrO_4^{2-} in simple simulant results in shifting the binding energy of the dominant

band to 530.2 eV with two shoulders at 531.9 eV and 533.5 eV. While the accurate assignment of these bands is difficult, the bands can be tentatively assigned based on literature reports. The 530.2 eV band is consistent with O 1s line corresponding to O-Ba lattice oxygen in a $BaCrO_4$ species and 531.9 eV matches O-H surface hydroxyl oxygen respectively.[66] However, these assignments have to be treated with caution suggesting the assignments are tentative at best, and other assignments are also possible.

Taken together, these structural characterization studies reveal that the structural frameworks of both anhydrous $BaSn(OH)_6$ and $Ba_2SnO_2(OH)_4$•$10H_2O$ decompose upon treatment of the **Ba-Sn** materials with either sulfate or chromate alkaline solutions due to formation of the thermodynamically more stable $BaSO_4$ or $BaCrO_4$ compounds.

Performance of the Ba-Sn materials toward sulfate uptake from AN-102 simulant

The performance of the **Ba-Sn** materials toward sulfate uptake was challenged under the AN-102 tank waste simulant conditions. AN-102 is considered a high-nitrate, medium sulfate level waste simulant.[12] The AN-102 simulant is a complex brine-like alkaline solution containing inorganic salts of predominantly sodium, aluminum, and potassium at their respective concentrations of about 5.1, 0.24 and 0.13 M. Among inorganic anions, nitrate (~1 M) and nitrite (~1.0 M) are the most concentrated followed by carbonate (~0.46 M) and free hydroxide (~0.35 M) (Table S.1). Sulfate and chromate are present at significantly lower concentrations of 94 mM and 12 mM, respectively. The concentration of the carbonate anion is about 4.9-5.4 times greater than that of sulfate which constitutes the largest challenge to the sequestration of sulfate in the form of $BaSO_4$.

This study utilized the same batch contact experimental protocol as for simple sulfate and chromate solutions described above. Approximately 25 mg of a **Ba-Sn** material was suspended

in 1 mL of AN-102 simulant and the time dependence of the uptake of SO_4^{2-} and CrO_4^{2-} was monitored by Raman spectroscopy. Both sulfate and chromate Raman bands are well-resolved from other spectral features allowing quantitative determination of these anions (Figure S7). To corroborate Raman results, AN-102 simulant samples treated with a representative **Ba-SnCl$_2$** material for 24 hrs were subjected to ICP-OES analysis, and excellent agreement between these two analytical methods was observed (Table 1).

All tested **Ba-Sn** materials performed similarly for sulfate uptake (Table 1) showing the robustness of this system. It was observed that 54 – 66 % of SO_4^{2-} is removed from the solution when solid-to-solution ratio is 25 mg/mL. This equates to a Ba:S molar ratio of approximately 1:1. The efficiency of the uptake appeared to be lower for both the anions in the AN-102 simulant than in the simple alkaline solutions (Figure 7, Table 1) with uptake values of 54% for both the chromate and sulfate after 24 hours which equates to a roughly 25% decrease in performance from a concentration standpoint. The 54 – 66% uptake for SO_4^{2-} is significant. A previous study[16] conducted on the waste solution from Hanford tank AN-107 which has a similar composition with high CO_3^{2-} concentration of 0.75 M and about 40 mM SO_4^{2-} demonstrated no precipitation of SO_4^{2-} with soluble $Ba(NO_3)_2$ salt even when it was added in five times molar excess in relation to SO_4^{2-} due to preferential precipitation of $BaCO_3$. A pretreatment step utilizing $Ca(NO_3)_2$ was necessary before acceptable uptake of SO_4^{2-} (about 55 – 70% depending on the Ba^{2+} quantity) was observed (Table 1). Thus, the present material would simultaneously require the addition of less mass and involve fewer process steps in the treatment of LAW prior to vitrification. The selective uptake of SO_4^{2-} over CO_3^{2-} with the present materials is attributed to the $SnO_2(OH)_2^{2-}$ moiety preferentially reacting with and is replaced by SO_4^{2-} over CO_3^{2-} due to lattice effects within the synthesized materials.

In comparison with the simple test solutions, the AN-102 simulant rate of uptake also appeared to be slower and following more complex kinetics for both anions. About 34 and 44% of the respective SO_4^{2-} and CrO_4^{2-} was removed from the solution within the first hour. For this initial uptake regime, the concentration of SO_4^{2-} or CrO_4^{2-} in the contact AN-102 simulant can be fit to a logarithmic behavior with respect to time, suggesting first order processes for their depletion. The first order kinetic rate constants, obtained from the plot's slope for the sorption of SO_4^{2-} and CrO_4^{2-} from the simulant solution are -1.60 x 10^{-4} sec^{-1} and -2.63 x 10^{-4} sec^{-1}, respectively, for the representative **Ba-SnO** material (Figure S8) suggesting faster reaction with CrO_4^{2-}. After one hour of contact, the uptake of SO_4^{2-} exhibited a gradual increase, however, it was not observed to reach equilibrium after 48 hours of monitoring. On the other hand, uptake of CrO_4^{2-} approached equilibrium within this time frame. This decrease of sorption rate and efficiency in AN-102 is most likely a consequence of the competing species in the matrix interfering with the uptake of SO_4^{2-} and CrO_4^{2-}. Despite this potential carbonate interference, the **Ba-Sn** materials are observed to exhibit a considerable affinity towards SO_4^{2-} and CrO_4^{2-}.

The performance of the **Ba-SnO** material was evaluated as a function of SO_4^{2-} concentration in the AN-102 matrix (27, 60, and 94 mM) at three different solid-to-liquid ratios of 12, 25 and 50 mg/mL (Figure 8). It was observed that SO_4^{2-} uptake increased nearly linearly with the increase of SO_4^{2-} concentration. The observation that for the same amount of composite, SO_4^{2-} uptake depends on the amount of total SO_4^{2-} present in solution suggests that other anions, e.g. carbonate, interfere with quantitative SO_4^{2-} uptake. Upon increasing SO_4^{2-} concentration, the SO_4^{2-} affinity of the composite presumably has a dominating effect driving the equilibrium towards higher uptake. Interestingly, the efficiency of the chromate uptake also increases with the increasing sulfate concentration suggesting that it could be related to the

incorporation of CrO_4^{2-} into $BaSO_4$ framework as suggested by the XRD results presented below. Sulfate uptake from AN-102 simulant containing 94 mM SO_4^{2-} increased with increasing solid-to-solution ratio. A similar trend is observed for CrO_4^{2-}.

The XRD analysis demonstrates that treatment of the **Ba-Sn** materials with the AN-102 simulant predominantly results in the formation of a $BaSO_4$ phase, with no crystalline phases corresponding to $BaCrO_4$ or $BaCO_3$ (Figures 1B, S9). This is indicative that treatment of the material with the AN-102 simulant results in the incorporation of CrO_4^{2-} and CO_3^{2-} as a replacement of the SO_4^{2-} ion in the $BaSO_4$ crystalline structure. Released Sn(IV) was at least partially converted to SnO_2.

Infrared spectroscopy of the **Ba-Sn** materials upon exposure to a complex simulant of AN-102 which contains both SO_4^{2-} and CrO_4^{2-}, shows a small signature at 422 cm^{-1} which had only previously been observed in the CrO_4^{2-} exposed material (Figures 2B, S4 – S6). Additionally, small peaks occur at 858, 880, 905, and 938 cm^{-1} which correspond to CrO_4^{2-}, showing that there is some uptake of CrO_4^{2-} by the material. However, examination of the IR spectrum also shows prominent peaks at 606, 634, and 1064 cm^{-1} and two broad overlapping peaks at approximately 1128, and 1178 cm^{-1}. These correspond closely to those of $BaSO_4$ and the sulfate exposed SO_4^{2-} material showing considerable uptake of SO_4^{2-} by the **Ba-Sn** materials in the complex AN-102 simulant.

Evaluation of the XPS spectra of the **Ba-SnO** material exposed to AN-102 simulant (Figure 4) suggests no change in the Ba $3d_{5/2}$ binding energy compared with the unexposed material. On the other hand, the chemical environment around the Sn center became comparatively electron deficient. The O 1s band exhibited a slight shift to higher energy and considerable narrowing indicative of a single environment presumably corresponding to the dominant $BaSO_4$ product. A comparison of the S $2p_{3/2}$ region for the **Ba-SnO** material exposed to the simple sulfate solution and

AN-102 simulant shows a shift towards a lower binding energy for the latter. This suggests a more electron rich S environment in the AN-102-exposed material, presumably consistent with a less hydrated SO_4^{2-} species due to the high ionic strength of the brine-like simulant matrix.

After exposure of the **Ba-Sn** materials to the AN-102 simulant the profile of TGA-DTA thermograms (Figures 6 bottom, S10 – S12) is significantly altered by comparison to the as synthesized material. The DTA profile is broad, and poorly defined over the entire range from 21 °C to 1096 °C. A mostly linear mass loss of only approximately 4 - 5 % is seen over the entire range suggesting that the integrity of the **Ba-Sn** materials exposed to the AN-102 simulant remains intact. Small continuous mass loss was attributed to the combination of the initial water loss and decomposition of $BaCO_3$ small quantity of which is expected to form upon **Ba-Sn** exposure the simulant. This drastic change in thermal behavior shows that a significant reaction has occurred with the simulant, suggesting uptake of SO_4^{2-}. Furthermore, after the AN-102 exposed material was heated during collection of the TGA-DTA, the material was reexamined by IR spectroscopy, and with exception of a slight broadening of the peaks between 1065 and 1178 cm^{-1} the spectrum remained little changed, demonstrating that $BaSO_4$ is formed preferentially to $BaCO_3$ and that the formed $BaSO_4$ is stable at temperatures which approximate those of the vitrification process.

Conclusions

The **Ba-Sn** materials can be easily synthesized via simple hydrothermal synthesis using various Sn(II/IV) precursors. Elemental and structural analyses indicated that the final product composition is insensitive to the oxidation state of the Sn precursor made within the specified pH range and contains $BaSn(OH)_6$ and the hydrates thereof. The ability of the synthesized **Ba-Sn**

materials to sequester SO_4^{2-} as $BaSO_4$ from the simulated tank waste solution and thermal stability of the obtained product up to 1100 °C, resembling the temperature range of the vitrification, was examined. It was observed that application of the **Ba-Sn** materials over a simple Ba^{2+} salt prevents formation of insoluble $BaCO_3$ prior to SO_4^{2-} sequestration. The efficient uptake of CrO_4^{2-} and $SO_4^{2-}$was observed in solutions containing large excess of CO_3^{2-}. This opens a pathway to selective uptake of SO_4^{2-} without the need to precipitate CO_3^{2-} in a separate process step. Structural characterization data suggests the mechanism of this sequestration is via the replacement of $SnO_2(OH)_2^{2-}$ in the crystal structure and subsequent solvation in the basic media. After exposure to the AN-102 tank waste simulant, analysis by TGA-DTA showed that the **Ba-Sn** materials retained the sequestered sulfate under temperatures relevant to the vitrification process. This proves that materials of the general formula $BaSn(OH)_6{\bullet}xH_2O$ are promising candidates for the selective sequestration of SO_4^{2-} in the tank waste solution prior to vitrification process, and hold promise for their application under the more complex chemistry present in a melter environment.

Based on the observed preferential formation of $BaSO_4$ in the presence of a large excess of carbonate, application of the **Ba-Sn** materials for the treatment of hazardous industrial aqueous effluents should be considered. This work provides a novel and practical approach to prepare functional inorganic nanomaterials for the separation or *in situ* sequestration of sulfate from aqueous solutions. Further testing is warranted to engineer the **Ba-Sn** materials for specific applications in column and/or batch sorption configurations.

Acknowledgements

The authors gratefully acknowledge the financial support provided by the U.S. Department of Energy, Office of River Protection,

Waste Treatment and Immobilization Plant Project. This research was performed at the Pacific Northwest National Laboratory operated by Battelle for the U.S. Department of Energy under Contract DE-AC05-76RL01830. Part of this research was performed at Environmental Molecular Sciences Laboratory, a national scientific user facility at Pacific Northwest National Laboratory managed by the Department of Energy's Office of Biological and Environmental Research. The authors would like to thank Dr. Vanessa E. Holfeltz for the many useful discussions and advice given throughout this work.

Table 1. Uptake of SO_4^{2-} and CrO_4^{2-} by the **Ba-Sn** materials measured by Raman spectroscopy at 24 hours equilibration time.

Material (25 mg)	**Simulant Composition (1 mL)**	**% SO_4^{2-} Uptake**	**% CrO_4^{2-} Uptake**
This work			
Ba-SnO	0.5 M NaOH, 1.11 M $NaNO_3$, 85 mM Na_2SO_4	83±2[a]	NA
	0.5 M NaOH, 1.11 M $NaNO_3$, 85 mM Na_2CrO_4	NA	81±2[a]
	AN-102 with 12 mM CrO_4^{2-}, 94 mM SO_4^{2-}	54±4[b]	55±4[b]
Ba-SnCl$_2$	0.5 M NaOH, 1.11 M $NaNO_3$, 85 mM Na_2SO_4	76±2[a]	NA
	0.5 M NaOH, 1.11 M $NaNO_3$, 85 mM Na_2CrO_4	NA	80±2[a]
	AN-102 with 12 mM CrO_4^{2-}, 94 mM SO_4^{2-}	54±5[c] 52±2[d]	66±5[c] 70±3[d]
Ba-SnCl$_{2/4}$	0.5 M NaOH, 1.11 M $NaNO_3$, 85 mM Na_2SO_4	78±2[a]	NA
	0.5 M NaOH, 1.11 M $NaNO_3$, 85 mM Na_2CrO_4	NA	81±2[a]
	AN-102 with 12 mM CrO_4^{2-}, 94 mM SO_4^{2-}	61± 2[e]	76± 2[e]
Ba-SnCl$_4$	0.5 M NaOH, 1.11 M $NaNO_3$, 85 mM Na_2SO_4	79±2[a]	NA
	0.5 M NaOH, 1.11 M $NaNO_3$, 85 mM Na_2CrO_4	NA	81±2[a]
	AN-102 with 12 mM CrO_4^{2-}, 94 mM SO_4^{2-}	66±2[a]	66±2[a]
Data taken from Fiskum et al., 2000.[16]			
$Ba(NO_2)_2$ at 31.3 mM[f]	AN-107 with 34 mM SO_4^{2}	6	NA
$Ba(NO_2)_2$ at 95.2 mM[f]		1	NA
0.7 M $Ca(NO_3)_2$ pre-strike followed by $Ba(NO_2)_2$ at 31.3 mM[g]		54	NA
0.7 M $Ca(NO_3)_2$ pre-strike followed by $Ba(NO_2)_2$ at 95.2 mM[g]		69	NA

[a] Standard deviation based on 10 different Raman measurements on the same sample.
[b] Standard deviation across four different batches of samples, each batch prepared and processed independently.
[c] Standard deviation across seven different batches of samples, each batch prepared and processed independently.
[d] ICP-OES analysis of the same samples performed to validate Raman quantitative measurements.
[e] Standard deviation across five different batches of samples, each batch prepared and processed independently.
[f] To a solution of 34 mM SO_4^{2-} in AN-107 simulant, measured amount of Ba^{2+} in the form of soluble $Ba(NO_2)_2$ was added.[16]
[g] The AN-107 sample was struck with appropriate amount of soluble Ca^{2+} salt to remove CO_3^{2-} present in the simulant prior to SO_4^{2-} removal. Subsequently, to a solution of 34 mM SO_4^{2-} present in the same AN-107 simulant solution, measured amount of Ba^{2+} in the form of soluble $Ba(NO_2)_2$ was added.[16]

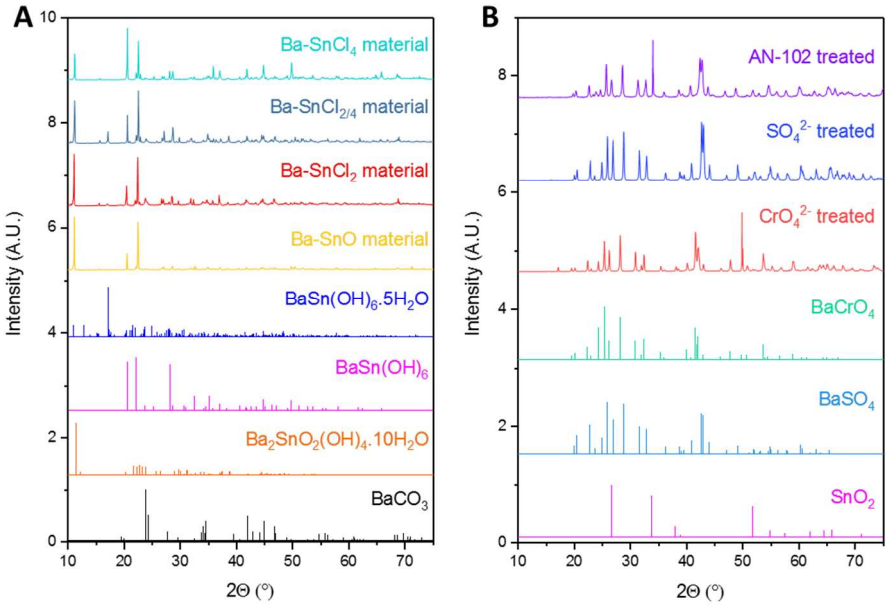

Figure 1. X-ray diffractograms of reference compounds and (A) the synthesized **Ba-Sn** materials and (B) **Ba-SnO** material exposed to the AN-102 simulated waste or 0.5 M NaOH/1.11 M $NaNO_3$ solutions containing 85 mM of Na_2SO_4 or Na_2CrO_4.

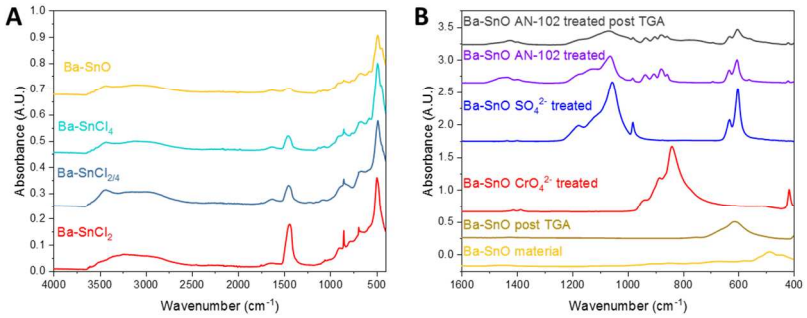

Figure 2. IR spectra of (A) the synthesized **Ba-Sn** materials and (B) **Ba-SnO** material exposed to the AN-102 simulated waste or 0.5 M NaOH/1.11 M $NaNO_3$ solutions containing 85 mM of Na_2SO_4 or Na_2CrO_4.

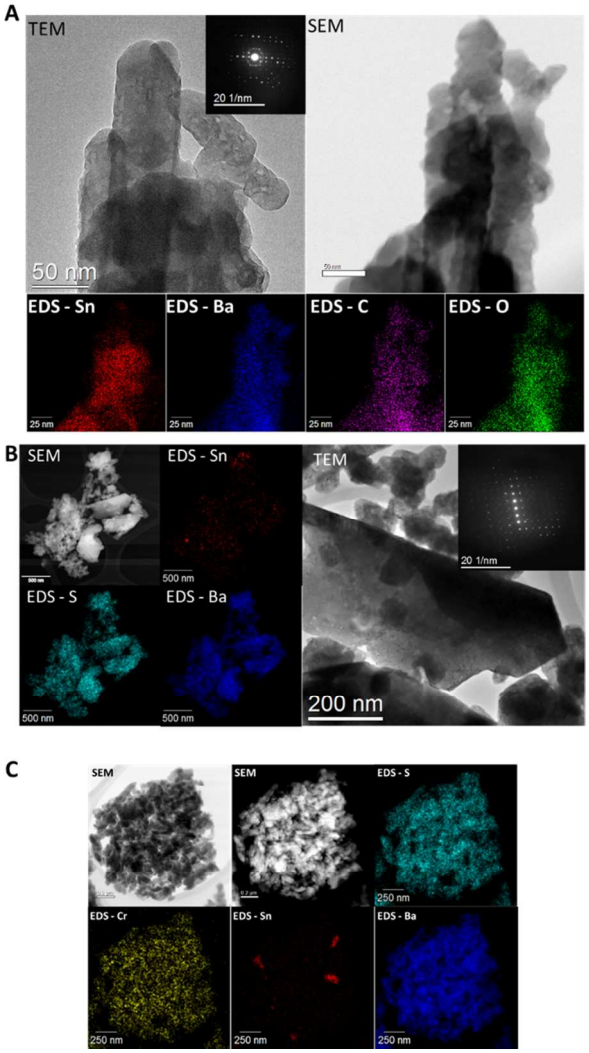

Figure 3. TEM and SEM images of the **Ba-SnO** material (A) as prepared showing crystalline nature of the material, (B) sulfate exposed to 85 mM Na_2SO_4 solution in 0.5 M NaOH/0.11 M $NaNO_3$, and (C) SEM images of the **Ba-SnO** material exposed to AN-102 simulant.

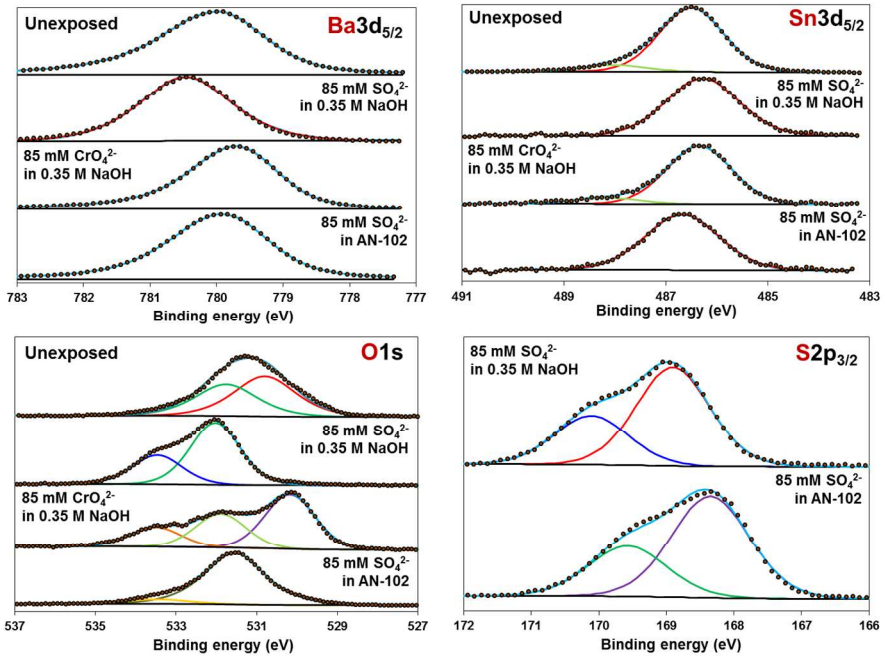

Figure 4. Solid state X-ray photoelectron spectra of Ba $3d_{5/2}$ (top left), Sn $3d_{5/2}$ (top right), O1s, and S $2P_{3/2}$ (bottom right) orbitals for the **Ba-SnO** material before and after exposure to the AN-102 simulated waste or 0.5 M NaOH/1.11 M $NaNO_3$ solutions containing 85 mM of Na_2SO_4 or Na_2CrO_4.

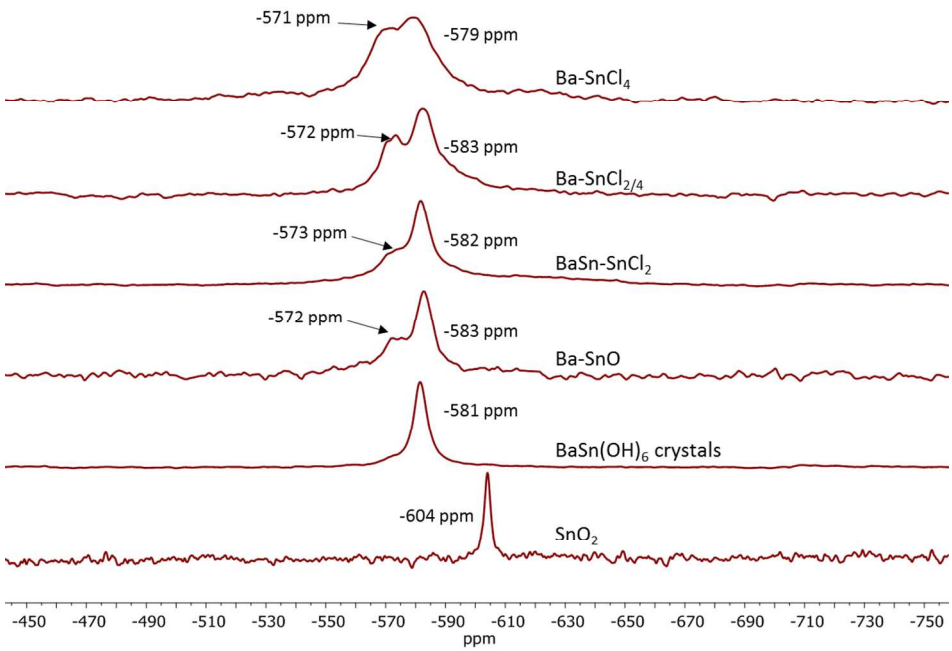

Figure 5. Spectral ^{119}Sn NMR layout of (from bottom to top) SnO_2, $BaSn(OH)_6$ crystals and **Ba-SnO**, **Ba-SnCl$_2$**, **Ba-SnCl$_{2/4}$**, and **Ba-SnCl$_4$** materials.

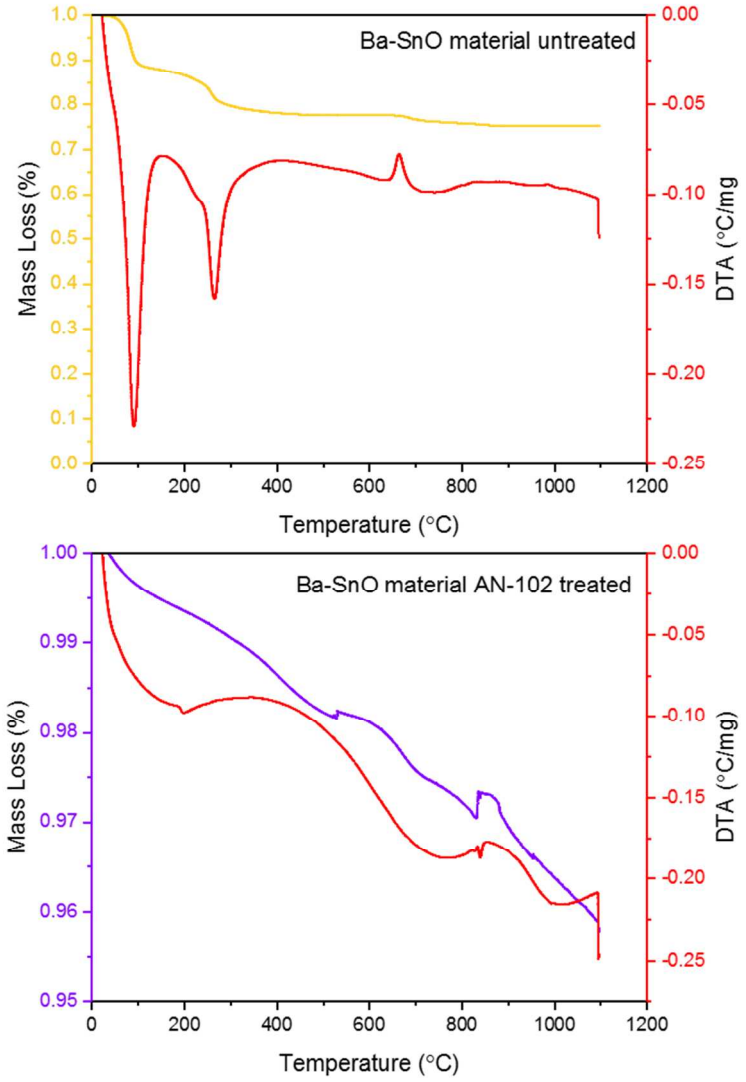

Figure 6. Thermogravimetric analysis and differential thermal analysis of the as synthesized **Ba-SnO** material (top) and after treatment with AN-102 simulant (bottom).

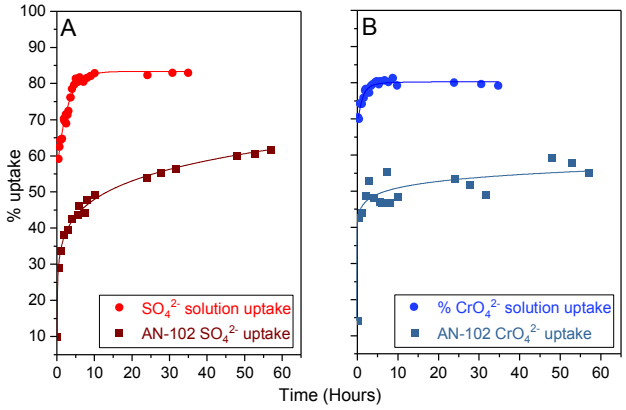

Figure 7. Uptake of SO_4^{2-} (A) and CrO_4^{2-} (B) from the AN-102 simulant or 0.5 M NaOH/1.11 M $NaNO_3$ solutions containing 85 mM of Na_2SO_4 or Na_2CrO_4 by the representative **Ba-SnO** material measured by reduction of the Raman intensity of the corresponding bands with time.

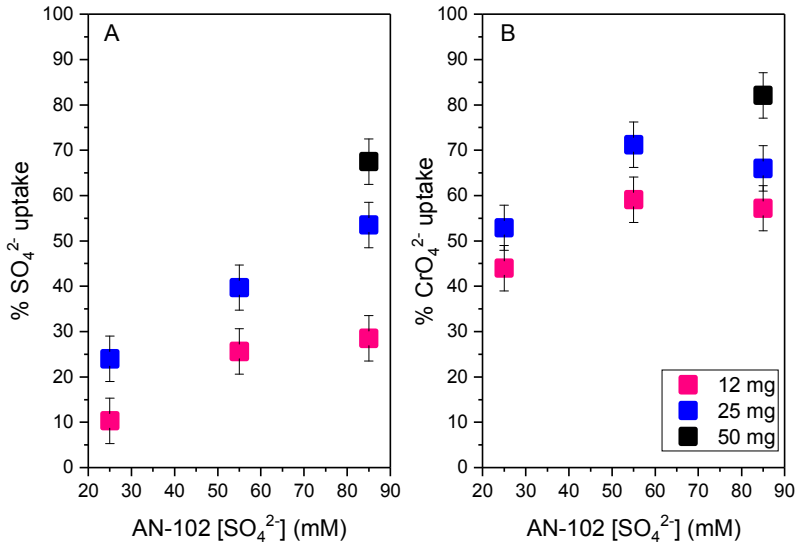

Figure 8. Effect of varying amount **Ba-SnCl$_2$** material and sulfate concentration in AN-102 simulant (1 mL) on the uptake of SO_4^{2-} (A) and CrO_4^{2-} (B).

References

(1) Silva, A. J.; Varesche, M. B.; Foresti, E.; Zaiat, M. *Process Biochem* **2002**, *37*, 927.

(2) Lens, P. N. L.; Visser, A.; Janssen, A. J. H.; Pol, L. W. H.; Lettinga, G. *Crit Rev Env Sci Tec* **1998**, *28*, 41.

(3) Kijjanapanich, P.; Annachhatre, A. P.; Esposito, G.; van Hullebusch, E. D.; Lens, P. N. L. *J Environ Manage* **2013**, *131*, 82.

(4) Dou, W. X.; Zhou, Z.; Jiang, L. M.; Jiang, A. J.; Huang, R. W.; Tian, X. C.; Zhang, W.; Chen, D. Q. *J Environ Manage* **2017**, *196*, 518.

(5) *Final Tank Closure and Waste Management Environmental Impact Statement for the Hanford Site, Richland, Washington* Office of River Protection, U.S. Department of Energy, 2012.

(6) Gollop, R. S.; Taylor, H. F. W. *Cement Concrete Res* **1996**, *26*, 1013.

(7) Taylor, H. F. W.; Famy, C.; Scrivener, K. L. *Cement Concrete Res* **2001**, *31*, 683.

(8) Glasser, F. P. *Cement Concrete Res* **1992**, *22*, 201.

(9) Myers, R. J.; Lothenbach, B.; Bernal, S. A.; Provis, J. L. *Appl Geochem* **2015**, *61*, 233.

(10) Vienna, J. D.; Kim, D. S.; Muller, I. S.; Piepel, G. F.; Kruger, A. A. *J Am Ceram Soc* **2014**, *97*, 3135.

(11) Jin, T. G.; Kim, D.; Tucker, A. E.; Schweiger, M. J.; Kruger, A. A. *J Non-Cryst Solids* **2015**, *425*, 28.

(12) Jin, T.; Kim, D.; Schweiger, M. J. In *Waste Management Conference* Phoenix, AZ, 2014.

(13) Hodgman, C. D.; Weast, R. C. *Handbook of Chemistry and Physics*; Rubber Pub. Co.: Ohio, USA, 1962.

(14) Kabdasli, I.; Tunay, O.; Orhon, D. *Water Sci Technol* **1995**, *32*, 21.

(15) Benatti, C. T.; Tavares, C. R. G.; Lenzi, E. *J Environ Manage* **2009**, *90*, 504.

(16) Fiskum, S. K.; Kurath, D. E.; Rapko, B. M. *Development and Demonstration of a Sulfate Precipitation Process for Hanford Waste Tank 241 -AN-107*, Pacific Northwest National Laboratory, 2000.

(17) Levitskaia, T. G.; Chatterjee, S.; Pence, N. K.; Romero, J.; Varga, T.; Engelhard, M. H.; Du, Y. G.; Kovarik, L.; Arey, B. W.; Bowden, M. E.; Walter, E. D. *Environ Sci-Nano* **2016**, *3*, 1003.

(18) Levitskaia, T. G.; Chatterjee, S.; Arey, B. W.; Campbell, E. L.; Hong, Y. C.; Kovarik, L.; Peterson, J. M.; Pence, N. K.; Romero, J.; Shutthanandan, V.; Schwenzer, B.; Varga, T. *Rsc Advances* **2016**, *6*, 76042.

(19) Chang, K.; Sun, Y. X.; Ye, F.; Li, X.; Sheng, G. D.; Zhao, D. L.; Linghu, W. S.; Li, H.; Liu, J. *Chem Eng J* **2017**, *325*, 665.

(20) Jawad, A.; Liao, Z. W.; Zhou, Z. H.; Khan, A.; Wang, T.; Ifthikar, J.; Shahzad, A.; Chen, Z. L.; Chen, Z. Q. *Acs Appl Mater Inter* **2017**, *9*, 28451.

(21) Koilraj, P.; Kamura, Y.; Sasaki, K. *Acs Sustain Chem Eng* **2017**, *5*, 9053.

(22) Wang, J.; Wang, P. Y.; Wang, H. H.; Dong, J. F.; Chen, W. Y.; Wang, X. X.; Wang, S. H.; Hayat, T.; Alsaedi, A.; Wang, X. K. *Acs Sustain Chem Eng* **2017**, *5*, 7165.

(23) Zhu, L.; Zhang, L. J.; Li, J.; Zhang, D.; Chen, L. H.; Sheng, D. P.; Yang, S. T.; Xiao, C. L.; Wang, J. Q.; Chai, Z. F.; Albrecht-Schmitt, T. E.; Wang, S. *Environ Sci Technol* **2017**, *51*, 8606.

(24) Theiss, F. L.; Ayoko, G. A.; Frost, R. L. *Appl Surf Sci* **2016**, *383*, 200.

(25) Yan, J.; Yang, Z. H. *J Appl Polym Sci* **2017**, *134*.

(26) Gupta, S.; Agarwal, D. D.; Banerjee, S. *Indian J Chem A* **2008**, *47*, 1004.

(27) Marcus, Y. *Ion Properties*; Marcel Dekker: New York, USA, 1997.

(28) Sranko, D.; Sipiczki, M.; Bajnoczi, E. G.; Daranyi, M.; Kukovecz, A.; Konya, Z.; Canton, S. E.; Noren, K.; Sipos, P.; Palinko, I. *J Mol Struct* **2011**, *993*, 62.

(29) Sranko, D.; Pallagi, A.; Kuzmann, E.; Canton, S. E.; Walczak, M.; Sapi, A.; Kukovecz, A.; Konya, Z.; Sipos, P.; Palinko, I. *Appl Clay Sci* **2010**, *48*, 214.

(30) Jeong, Y.; Yum, W. S.; Jeon, D.; Oh, J. E. *Cement and Concrete Composites* **2017**, *79*, 34.

(31) Mobasher, N.; Bernal, S. A.; Hussain, O. H.; Apperley, D. C.; Kinoshita, H.; Provis, J. L. *Cement Concrete Res* **2014**, *66*, 64.

(32) Mobasher, N.; Kinoshita, H.; Bernal, S. A.; Sharrard, C. A. *Adv Appl Ceram* **2014**, *113*, 460.

(33) Buscaglia, M. T.; Leoni, M.; Viviani, M.; Buscaglia, V.; Martinelli, A.; Testino, A.; Nanni, P. *J Mater Res* **2003**, *18*, 560.

(34) Mizoguchi, H.; Bhuvanesh, N. S. P.; Kim, Y. I.; Ohara, S.; Woodward, P. M. *Inorg Chem* **2014**, *53*, 10570.

(35) Kamaha, S.; Reuter, H. *Z Anorg Allg Chem* **2009**, *635*, 2058.

(36) Byrappa, K.; Yoshimura, M. *Handbook of Hydrothermal Technology*; William Andrew Publishing: New York, 2001.

(37) Nyquist, R. A.; Kagel, R. O. *Handbook of infrared and raman spectra of inorganic compounds and organic salts: infrared spectra of inorganic compounds*; Academic Press Inc.: New York, New York, USA, 2012.

(38) Wu, X. H.; Lv, G.; Hu, X. Y.; Tang, Y. W. *J Nanomater* **2012**.

(39) Lu, W. S.; Schmidt, H. *Adv Powder Technol* **2008**, *19*, 1.

(40) Grimvall, S. *Acta Chem Scand A* **1982**, *36*, 309.

(41) Chen, X. Y.; Grandbois, M. *J Raman Spectrosc* **2013**, *44*, 501.
(42) *Atlas of Eh-pH diagrams*, National Institute of Advanced Industrial Science and Technology, Research Center for Deep Geological Environments, 2005.
(43) Andrews, L.; Wang, X. F. *Inorg Chem* **2005**, *44*, 11.
(44) Wang, X. F.; Andrews, L. *J Phys Chem A* **2005**, *109*, 9013.
(45) Pasierb, P.; Komornicki, S.; Rokita, M.; Rekas, M. *J Mol Struct* **2001**, *596*, 151.
(46) Kloprogge, J. T.; Wharton, D.; Hickey, L.; Frost, R. L. *Am Mineral* **2002**, *87*, 623.
(47) Zhong, F. L.; Zhuang, H. Q.; Gu, Q.; Long, J. L. *Rsc Advances* **2016**, *6*, 42474.
(48) Sharma, N.; Shaju, K. M.; Rao, G. V. S.; Chowdari, B. V. R. *J Power Sources* **2005**, *139*, 250.
(49) Suzer, S.; Voscoboinikov, T.; Hallam, K. R.; Allen, G. C. *Fresen J Anal Chem* **1996**, *355*, 654.
(50) Shuttleworth, D. *J Phys Chem-Us* **1980**, *84*, 1629.
(51) Golestanifard, F.; Hashemi, T.; Mackenzie, K. J. D.; Hogarth, C. A. *J Mater Sci* **1983**, *18*, 3679.
(52) Kwoka, M.; Ottaviano, L.; Passacantando, M.; Santucci, S.; Czempik, G.; Szuber, J. *Thin Solid Films* **2005**, *490*, 36.
(53) Gu, Q.; Long, J. L.; Zhou, Y. G.; Yuan, R. S.; Lin, H. X.; Wang, X. X. *J Catal* **2012**, *289*, 88.
(54) Huang, H. W.; Lin, J. J.; Fan, L. Z.; Wang, X. X.; Fu, X. Z.; Long, J. L. *J Phys Chem C* **2015**, *119*, 10478.
(55) Gu, Q.; Long, J. L.; Fan, L. Z.; Chen, L. M.; Zhao, L. L.; Lin, H. X.; Wang, X. X. *J Catal* **2013**, *303*, 141.
(56) Wang, H. J.; Sun, F. Q.; Zhang, Y.; Li, L. S.; Chen, H. Y.; Wu, Q. S.; Yu, J. C. *J Mater Chem* **2010**, *20*, 5641.
(57) Clayden, N. J.; Dobson, C. M.; Fern, A. *J Chem Soc Dalton* **1989**, 843.

(58) Tunstall, D. P.; Patou, S.; Liu, R. S.; Kao, Y. H. *Mater Res Bull* **1999**, *34*, 1513.

(59) Kutty, T. R. N.; Vivekanadan, R. *Mater Res Bull* **1987**, *22*, 1457.

(60) *Spectral Database for Organic Compounds (SDBS); infrared spectrum (#40053)*, 2017.

(61) Japa, M.; Panoy, P.; Anuchai, S.; Phanichphant, S.; Nimmanpipug, P.; Kaowphong, S.; Tantraviwat, D.; Inceesungvorn, B. *Rsc Advances* **2016**, *6*, 1571.

(62) *Spectral Database for Organic Compounds (SDBS): infrared spectrum (#40201)*, 2017.

(63) Christie, A. B.; Lee, J.; Sutherland, I.; Walls, J. M. *Appl Surf Sci* **1983**, *15*, 224.

(64) Allen, G. C.; Curtis, M. T.; Hooper, A. J.; Tucker, P. M. *J Chem Soc Dalton* **1973**, 1675.

(65) Contarini, S.; Rabalais, J. W. *J Electron Spectrosc* **1985**, *35*, 191.

(66) Contarini, S.; Aduru, S.; Rabalais, J. W. *J Phys Chem-Us* **1986**, *90*, 3202.

TOC Graphics

Novel functional **Ba-Sn** nanomaterials for separation or *in situ* sequestration of sulfate from complex aqueous carbonate solutions were developed.